01 Jun 2014

Nondestructive Evaluation of Mechanically Stabilized Earth Walls with Frequency-Modulated Continuous Wave (FM-CW) Radar

Mohammad Tayeb Ahmad Ghasr
Missouri University of Science and Technology, mtg7w6@mst.edu

Yi Bao

Kuang Ying

K. M. Combs

et. al. For a complete list of authors, see https://scholarsmine.mst.edu/ele_comeng_facwork/3388

MID-AMERICA
TRANSPORTATION CENTER

Report # MATC-MS&T: 196

Final Report
WBS:25-1121-0003-196

Nondestructive Evaluation of Mechanically Stabilized Earth Walls with Frequency-Modulated Continuous Wave (FM-CW) Radar

Genda Chen, Ph.D., P.E., F .ASCE, F .Sei
Professor and Robert W. Abbett Distinguished Chair in Engineering
Department of Civil, Architectural, and Environmental Engineering
Missouri University of Science and Technology

Reza Zoughi, Ph.D.

K. Ying

K.M. Combs

M.T. Ghasr

Y. Bao

2014

A Coopertative Research Project sponsored by
U.S. Department of Tranportation-Research, Innovation and Technology Innovation Administration

Nondestructive Evaluation of Mechanically Stabilized Earth Walls with Frequency-Modulated Continuous Wave (FM-CW) Radar

G.D. Chen, Ph.D., P.E., F.ASCE, F.SEI
Professor and Abbett Distinguished Chair in Civil Engineering
Department of Civil, Architectural, and Environmental Engineering
Missouri University of Science and Technology

R. Zoughi, Ph.D.
Schlumberger Distinguished Professor
Department of Electrical and Computer Engineering
Missouri University of Science and Technology

M.T. Ghasr, Ph.D.
Research Assistant Professor
Department of Electrical and Computer Engineering
Missouri University of Science and Technology

Y. Bao, Ph.D. Candidate
Graduate Research Assistant
Department of Civil, Architectural, and Environmental Engineering
Missouri University of Science and Technology

K. Ying
Undergraduate Student Research Assistant
Department of Electrical and Computer Engineering
Missouri University of Science and Technology

K.M. Combs
Undergraduate Student Research Assistant
Department of Electrical and Computer Engineering
Missouri University of Science and Technology

A Report on Research Sponsored by

Mid-America Transportation Center

University of Nebraska–Lincoln

June 2014

Technical Report Documentation Page

1. Report No. 25-1121-0003-196	2. Government Accession No.	3. Recipient's Catalog No.
4. Title and Subtitle Nondestructive Evaluation of Mechanically Stabilized Earth Walls with Frequency-Modulated Continuous Wave (FM-CW) Radar		5. Report Date June 2014
		6. Performing Organization Code
7. Author(s) M.T. Ghasr, Y. Bao, K. Ying, K.M. Combs, R. Zoughi, and G.D. Chen		8. Performing Organization Report No. 25-1121-0003-196
9. Performing Organization Name and Address Mid-America Transportation Center 2200 Vine St. PO Box 830851 Lincoln, NE 68583-0851		10. Work Unit No. (TRAIS)
		11. Contract or Grant No.
12. Sponsoring Agency Name and Address Research and Innovative Technology Administration 1200 New Jersey Ave., SE Washington, D.C. 20590		13. Type of Report and Period Covered Final Report, July 1 2012 - June 20 2014
		14. Sponsoring Agency Code MATC TRB RiP No. 17139
15. Supplementary Notes		

16. Abstract

Effective techniques for a nondestructive evaluation of mechanically stabilized earth (MSE) walls during normal operation or immediately after an earthquake event are yet to be developed. MSE walls often have a rough surface finishing for the purpose of decoration and are reinforced with both horizontal and vertical steel bars. Two wide-band microwave inspection approaches were investigated for detecting and evaluating characteristics of materials behind an MSE wall section. The first approach used spot measurements with a wide-band frequency-modulated continuous wave (FM-CW) radar system. While effective to penetrate through mortar blocks in the laboratory, the radar system was found to have limited applications in MSE walls due to its thick layer, material heterogeneity, surface roughness, and the presence of steel bars. The second approach took wide-band measurements on a two-dimensional (2D) grid and produced three-dimensional (3D) images using a synthetic aperture radar algorithm. Imaging allows for signal averaging and relatively easy distinction of localized features such as steel bars from undesired flaws. Two-dimensional slice images at the location of the anomalies were produced. Several different anomalies placed behind the wall can be detected, demonstrating the effectiveness of the imaging technique as a potential approach for back-fill soil inspection (e.g., moisture, void) behind an MSE wall.

17. Key Words	18. Distribution Statement		
19. Security Classif. (of this report) Unclassified	20. Security Classif. (of this page) Unclassified	21. No. of Pages 30	22. Price

Table of Contents

List of Figures

Acknowledgements

Financial support for this study was provided by the Mid-America Transportation Center under Contract Agreement No. 25-1121-0003-196. The authors would like to thank Jason Cox and John Bullock for their assistance with various experimental setups.

Disclaimer

The contents of this report reflect the views of the authors, who are responsible for the facts and the accuracy of the information presented herein. This document is disseminated under the sponsorship of the U.S. Department of Transportation's University Transportation Centers Program, in the interest of information exchange. The U.S. Government assumes no liability for the contents or use thereof.

Abstract

Effective techniques for a nondestructive evaluation of mechanically stabilized earth (MSE) walls during normal operation or immediately after an earthquake event are yet to be developed. MSE walls often have a rough surface finishing for the purpose of decoration and are reinforced with both horizontal and vertical steel bars. Two wide-band microwave inspection approaches were investigated for detecting and evaluating characteristics of materials behind an MSE wall section. The first approach used spot measurements with a wide-band frequency-modulated continuous wave (FM-CW) radar system. While effective to penetrate through mortar blocks in the laboratory, the radar system was found to have limited applications in MSE walls due to its thick layer, material heterogeneity, surface roughness, and the presence of steel bars. The second approach took wide-band measurements on a two-dimensional (2D) grid and produced three-dimensional (3D) images using a synthetic aperture radar algorithm. Imaging allows for signal averaging and relatively easy distinction of localized features such as steel bars from undesired flaws. Two-dimensional slice images at the location of the anomalies were produced. Several different anomalies placed behind the wall can be detected, demonstrating the effectiveness of the imaging technique as a potential approach for back-fill soil inspection (e.g., moisture, void) behind an MSE wall.

Executive Summary

This research project was focused on the exploration of microwave technology as a potential inspection tool for mechanically stabilized earth (MSE) walls that are widely used in highway bridge approaches. MSE walls have a rough surface finishing for decorative purposes and are reinforced with both horizontal and vertical steel bars. The main objectives of this study were: (1) to quantify the laboratory performance and ability of a wide-band, portable frequency-modulated continuous-wave (FM-CW) radar system for the detection of defects behind MSE walls; and (2) to demonstrate the field applicability and performance of the existing radar system for the field inspection of MSE walls. Two inspection methods were investigated in this study.

The first inspection method involved wide-band microwave spot measurements along with an inverse fast Fourier transform (FFT) algorithm for detecting and evaluating the characteristics of materials behind an MSE wall section. Initially a relatively high-frequency and wide-band FM-CM radar system was used. It operated in the 8-18 GHz range and provided high spatial and along-depth resolution. While effective to penetrate through mortar blocks in the laboratory, the radar system was found to have limited applications in MSE walls due to its thick layer, material heterogeneity, surface roughness and the presence of steel bars. Subsequently, time-domain reflectometry, which is equivalent to FM-CW radar, was employed with promising test results. The operating frequency for the time-domain reflectometry ranged from 1 to 6 GHz, which is much lower than that of the FM-CW radar and hence has better signal penetration capability. Even so, the presence of steel bars and surface roughness of walls determined that "spot type" measurements may only provide limited unambiguous measurement data/results for the inspection of an MSE wall section.

The second inspection method involved wide-band measurements on a two-dimensional (2D) grid (raster scanning) and produced three-dimensional (3D) images using a synthetic

aperture radar (SAR) algorithm. Raster scanning allows for signal averaging and relatively easy distinction of localized features such as steel bars from undesired flaws. To this end, a wide-band laboratory imaging system (1-4 GHz) was employed along with advanced SAR imaging algorithms to generate 2D slice images of a wall at various depths. By estimating and subtracting the wall surface scattering from the images, several different anomalies placed behind the wall can be detected, demonstrating the effectiveness of the imaging technique as a potential approach for back-fill soil inspection (e.g., moisture, void) behind an MSE wall. The surface scattering (baseline) can be estimated from the same panel prior to void development and stored for future use. Having a history of the wall panel is also helpful in wall deterioration monitoring such as the corrosion of reinforcing bars. Alternatively, the surface scattering can be estimated from neighboring panels in excellent conditions. For MSE walls that do not have any decorative surface features, this method provides better imaging capabilities.

The imaging technique also allows for distinguishing voids from water by monitoring the reflected signal strength. Voids produce less reflection compared to sand and water and appear as dark spots in the image. Water produces a stronger reflection and appears as bright spots in the image. Further studies are required to bring the technique into field applications.

An imaging system with a scanning platform can be designed to be portable for field applications. The use of a scanning platform that spans two adjacent wall panels can produce differential detection capabilities, further enhance the signal to clutter ratio, and potentially provide high detection probability. The microwave SAR imaging technique is robust and does not require any prior knowledge of MSE wall structures except for the thickness of walls.

Chapter 1 Introduction

Mechanically Stabilized Earth (MSE) walls have recently received increasing applications in transportation infrastructure. The advantages of MSE walls are primarily cost, rate of construction, and tolerance to settlement. MSE walls are widely used in the high elevation approach of highway bridges. Their stability directly affects the integrity of the bridge approach and thus threatens the safety of passengers if an unstable situation arises. Therefore, the proposed work is directly related to the USDOT Strategic Goal: enhancing safety. In addition, a robust NDE method can provide a potential technique for the condition assessment of MSE stability before a retrofit strategy is developed. As such, the proposed work is also relevant to the USDOT Strategic Goal: improving the state of good repair. Based on the field observations during the 2010 Chile Earthquake, the performance of MSE walls under earthquake loads exceeded the expectation by AASHTO standard (AASHTO, 2008). Therefore, their applications are expected to be expanded in the near future. However, cost-effective nondestructive evaluation (NDE) techniques for MSE wall inspections, either during the normal operation or after an extreme event, are yet to be developed.

In this study, two distinct NDE techniques were implemented to evaluate the condition of back-fill materials behind MSE wall panels, namely: frequency-modulated continuous-wave (FM-CW) radar and the wideband synthetic aperture radar (SAR) imaging technique. The engineering parameters interesting to field inspections include, but are not limited to, voids and appreciable changes in the water/moisture content behind a MSE wall. The former technique produces high-range resolution in the depth direction and high spatial resolution on the wall surface with a relatively small inspection footprint. The latter technique is a robust and well-developed imaging methodology capable of producing high resolution images in all three directions (two in-plane and one out-of-plane directions of a wall).

This report describes an MSE wall used in these investigations, the two nondestructive (NDE) techniques, and the findings and pertinent discussion of the obtained results. It consists of four main sections. Chapter 1 introduces the background information and emphasizes the importance of this research. Chapter 2 details the test setup, the measurement procedure and methodology, the test results, and the discussion. Chapter 3 summarizes all the findings and conclusions.

Chapter 2 Experimental Investigation

2.1 Test Bed

As shown in figure 2.1, a 5ft × 5ft × 7in (full size) reinforced concrete MSE wall panel (TENSAR Int.) was used in this study. It was reinforced with #4 epoxy-coated steel bars that were 0.5 in. in minimum diameter and located approximately at its middle depth. The concrete used in the construction of panels was Class A-1, 4 ksi compressive strength, which contained both fine and coarse aggregates. The size of the coarse aggregates was up to 1 in. The wall panel had a 2 in. rugged decoration layer on the front side.

Figure 2.1 Erected MSE wall used in this investigation

During testing, all MSE walls were supported on wood blocks to minimize electromagnetic interference (EMI). An erected panel in the application position is shown in figure 2.1, in which the orthogonal white lines represent the location of reinforcement bars embedded in the concrete. To provide a uniform scanning distance, a piece of foam (2 in. thick) was attached on the decorative face, as indicated in figure 2.2.

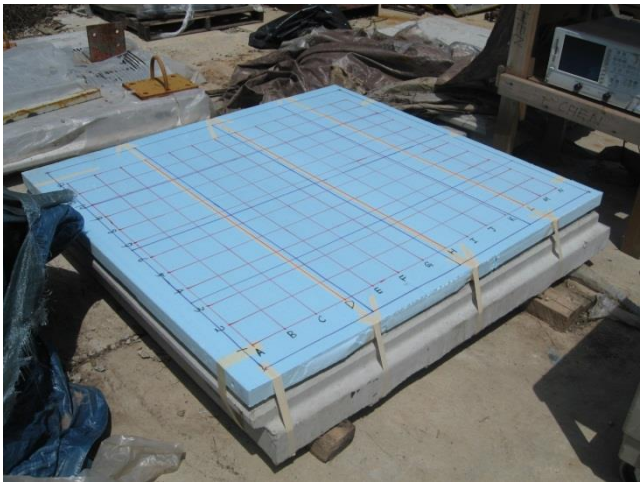

Figure 2.2 Construction foam (blue) on the decorative face of the wall to produce a uniform scanning/measurement distance

2.2 Frequency-modulated Continuous Wave (FM-CW) Radar

One well-established microwave technique for determining distance or boundary locations between different materials (e.g., retaining wall and back-filled soil or a void, etc.) and to perform remote sensing is the use of a frequency-modulated continuous-wave (FM-CW) radar system [1-3]. For MSE wall inspections, such a radar can measure the distance between the outside surface of the wall and the backfill soil, and any additional boundaries that may exist such as large voids behind the wall or changes in the properties of the soil (e.g., wet, dry, etc.). In addition, the amplitude of the reflected signals at various boundaries give information about material property differences on either side of the boundary. The FM-CW radar has several attractive features [1]: it has a relatively simple microwave hardware, a low microwave power requirement (in the milliwatt range), a low frequency radar output range (tens of KHz), it is compact, portable, and a versatile package, and it continuously monitors wall thickness and boundary location.

Figure 2.3 shows the general schematic of an FM-CW radar system. The modulator produces a triangular (or a linear ramp) waveform. A portion of the modulated signal is then sent to the local oscillator (LO) port of the mixer, using a directional coupler, while the remaining portion passes through a circulator and is then transmitted via the antenna. This signal travels through the wall and is partially reflected back from boundaries behind the wall, received by the antenna, sent through the circulator, and fed to the radio frequency (RF) port of the mixer. The reference signal at the LO port and this reflected signal at the RF port are then "mixed" to produce a low frequency signal at the intermediate frequency (IF) port of the mixer, which is proportional to the delay introduced in the reflected signal due to its two-way travel to the end of the wall and back (i.e., range or distance). Consequently, the frequency at which the signal appears at the IF port can be measured from a spectrum analyzer or a simple tracking filter and is *directly* related to the distance of the target.

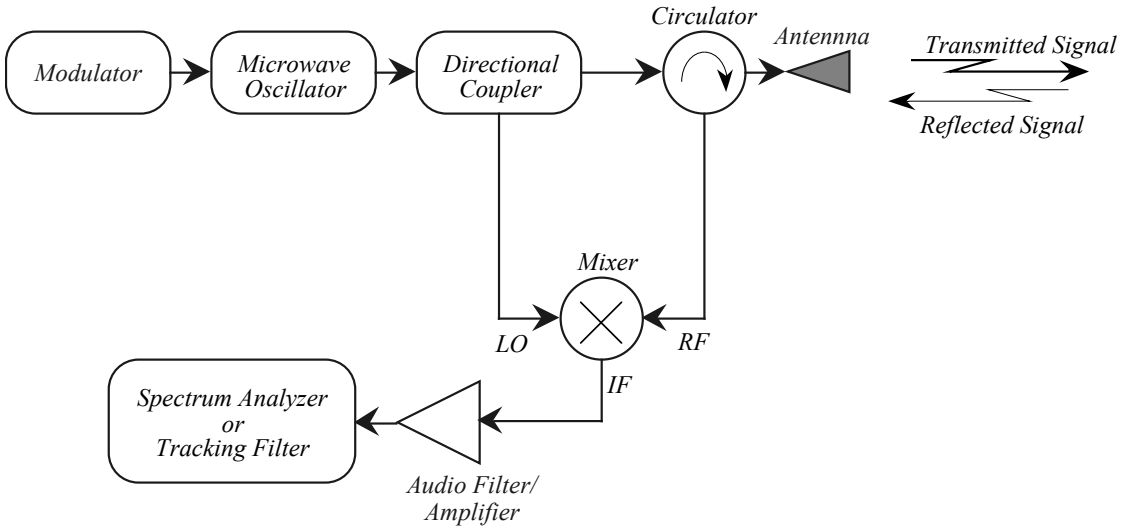

Figure 2.3 The general schematic of an FM-CW radar system

The important parameters that affect the determination of wall thickness include:

modulation frequency, transmitted signal bandwidth, range or distance to the target, permittivity of the material, range resolution, and range frequency.

The objectives of using an FM-CW radar system were: (1) to be able to quantify the laboratory performance and ability of an existing wide-band portable frequency-modulated continuous-wave (FM-CW) radar system for detection of anomalies behind mechanically stabilized earth (MSE) walls, and (2) to demonstrate the field applicability and performance of this type of radar system for the field inspection of MSE walls. To this end, an 8-18 GHz FM-CW radar that was previously built for the purpose of testing ceramic refractory bricks was employed. This radar was further modified and its characteristics were improved to enhance its portability and dynamic range by performing the following steps:

1. Rearranged the location of the source to be directly attached to the RF circuitry, hence eliminating cable losses. Consequently, the existing power amplifier was removed leading to a reduction in power consumption.
2. The RF switch was moved from the source side to the antenna side. This enabled the functionality of the automatic calibration check.
3. The circulator was replaced by a directional coupler to obtain a better wideband response.
4. The power supply was replaced by a small desktop power brick to increase portability.
5. A new ABS plastic case was machined to house the newly modified handheld FM-CW radar.
6. The radar control software was also updated and rewritten to facilitate improved data save/recall capabilities and provide self-testing.

Figure 2.4 shows the modified FM-CW radar circuitry before packaging. Figure 2.5 shows the ABS-packaged FM-CW radar with a high gain antenna attached. Figure 2.6 shows the

application of the FM-CW radar for finding interfaces between refractory bricks. In the graph shown, each peak represents an interface. The reflection from the horn-air interface is removed by measuring this reflection when radiating into air and subsequently subtracting it from any consequent measurements.

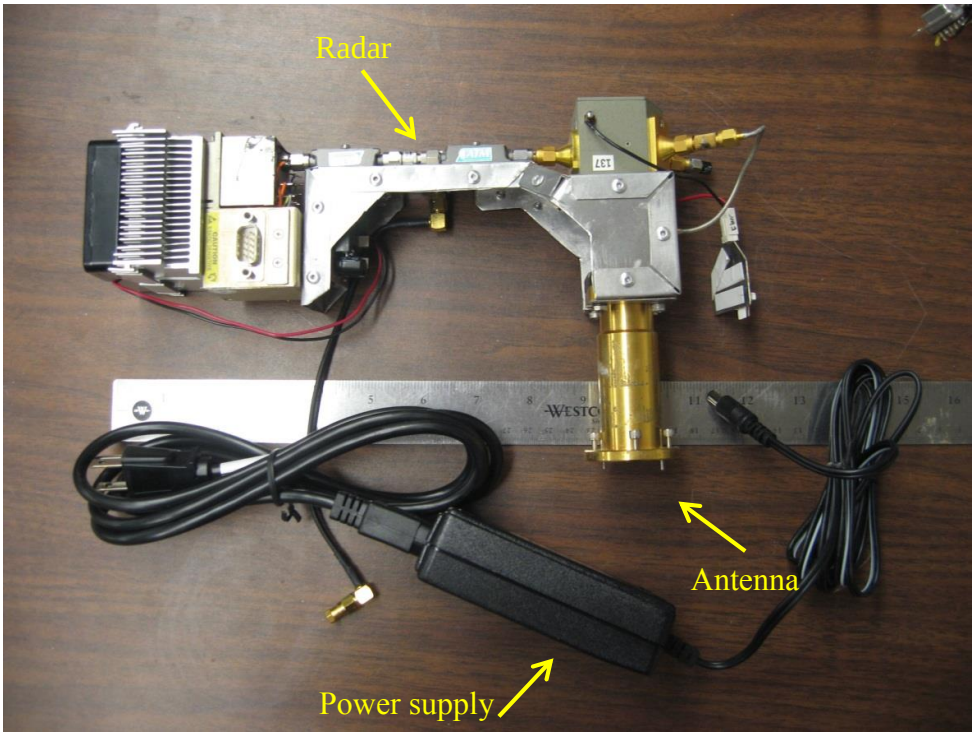

Figure 2.4 The modified FM-CW radar circuitry prior to packaging

Figure 2.5 ABS-packaged FM-CW radar with a high-gain horn antenna

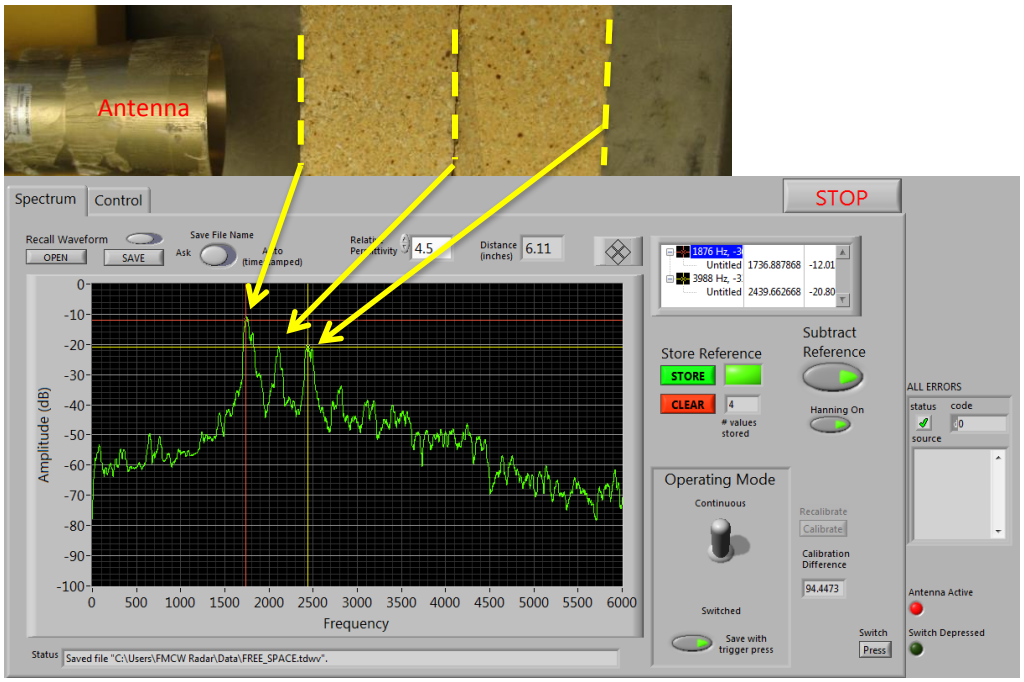

Figure 2.6 Using the FM-CW radar to find interfaces in-between refractory bricks; each peak represents a dielectric interface

Figure 2.7 shows the results from a laboratory test performed using two 4”-thick concrete slabs with the FM-CW radar. In this test, the FM-CW radar shows the capability of detecting voids through a 4”-thick slab of concrete. However, the high signal loss associated with the concrete slab significantly attenuates the microwave signal to a great extent. Consequently, the

peaks representing the back wall and the far side of the void are quite faint when compared to the background clutter (other peaks). This experiment showed that because this particular FM-CW radar operates at relatively high frequencies (8-18 GHz), it may suffer from such signal attenuations when used on a thick MSE wall. To further assess the signal attenuation issue, a time-domain reflectometry experiment was performed using an Agilent 8753E vector network analyzer (VNA) and a wideband (1-4 GHz) horn antenna. This experiment is similar to the one using the FM-CW radar, however in this case, a lower frequency range was used. Signal attenuation through materials decreases as the operating frequency decreases. This setup was used to detect an air gap behind an 8”-thick concrete block, as shown in figure 2.8. As indicated by the various arrows pointing to the peaks in the graphs, this setup was capable of detecting a void behind the 8”-thick concrete block. Furthermore, due to the lower operating frequency range and the lower signal attenuation, the peaks resulting from the void are distinguishable from background clutter. The drawback of this setup is the smaller bandwidth of the system (3 GHz) that results in a lower than desirable range resolution. To obtain a higher range resolution, an antenna capable of operating in a wider frequency band may be used, such as a Vivaldi antenna. Figure 2.9 shows a 1-6 GHz Vivaldi antenna being used to detect a void behind a retaining wall section. The smaller concrete blocks behind the wall were used to create a 4”-thick gap. The test results are shown in figure 2.10. The Agilent 8753E VNA was also used to make these measurements. The results show that this system is capable of detecting the front and back interface of the wall. It is also capable of detecting a metallic plate (strong reflector) placed 4” behind the wall. However, when detecting the small concrete block from a 4” distance, the signal peak becomes weak and fades into the background clutter. It must be noted that this MSE wall section is an inhomogeneous medium with an uneven surface, a large aggregate, and a mesh

of rebars that significantly limit microwave signal penetration. Also, all of these factors cause signal scattering that further results in signal loss and additional clutter. Overall, using an FM-CW radar or time-domain reflectometery proved to be an unreliable solution for detecting voids behind such structures. Consequently, an alternative solution was implemented involving wideband synthetic aperture radar (SAR) imaging, as described in the next section.

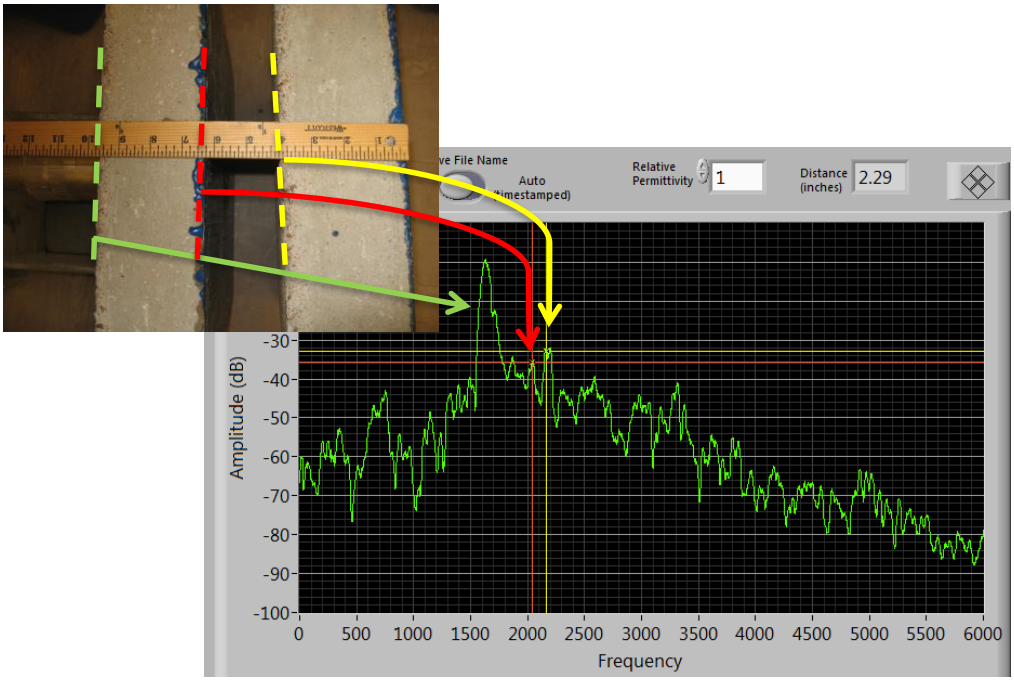

Figure 2.7 Testing the 8-18 GHz FM-CW radar on two concrete slabs in the laboratory

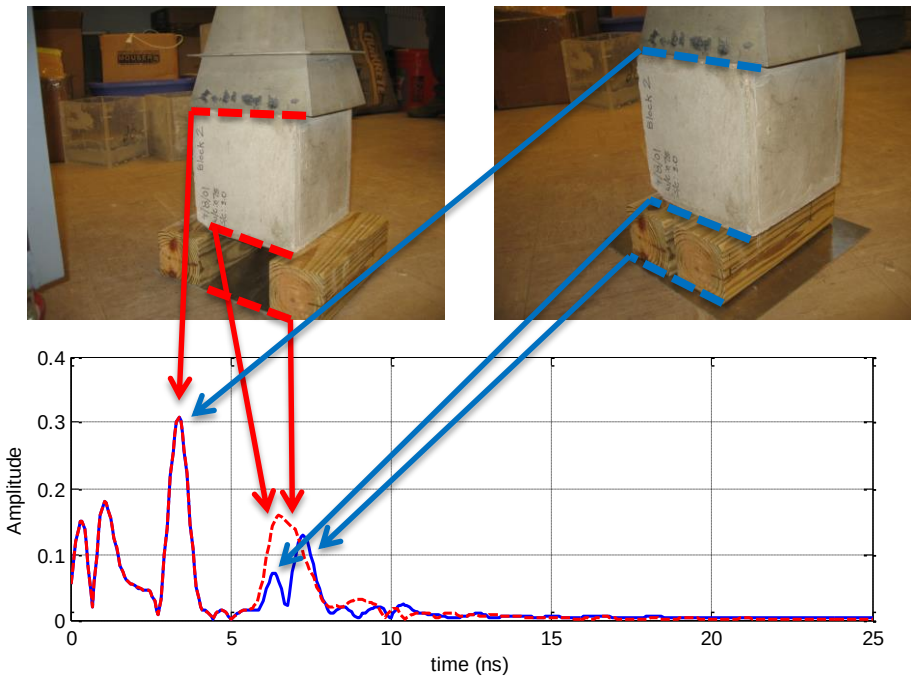

Figure 2.8 Time-domain reflectometry results from an 8”-thick concrete block using a VNA and a wideband (1-4 GHz) antenna

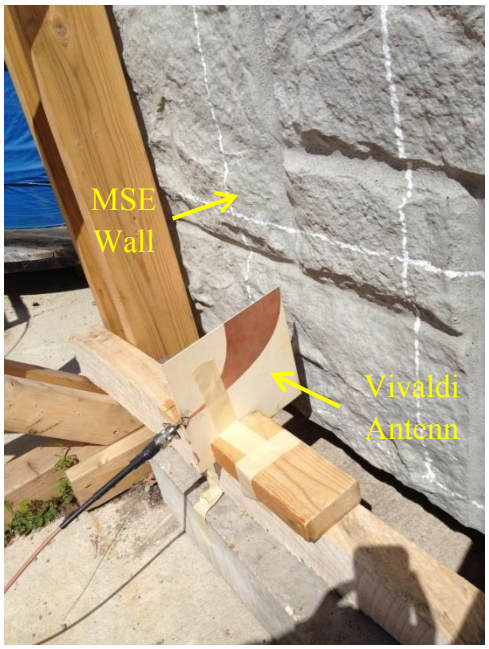

(a)

(b)

(c)

Figure 2.9 Using a wideband (1-6 GHz) Vivaldi antenna to perform time-domain reflectometery on an MSE wall section, which shows (a) the front of the wall with the Vivaldi antenna, (b) the back of the wall with concrete blocks creating a 4” gap, and (c) the back of the wall with concrete blocks firm against the wall (no gap)

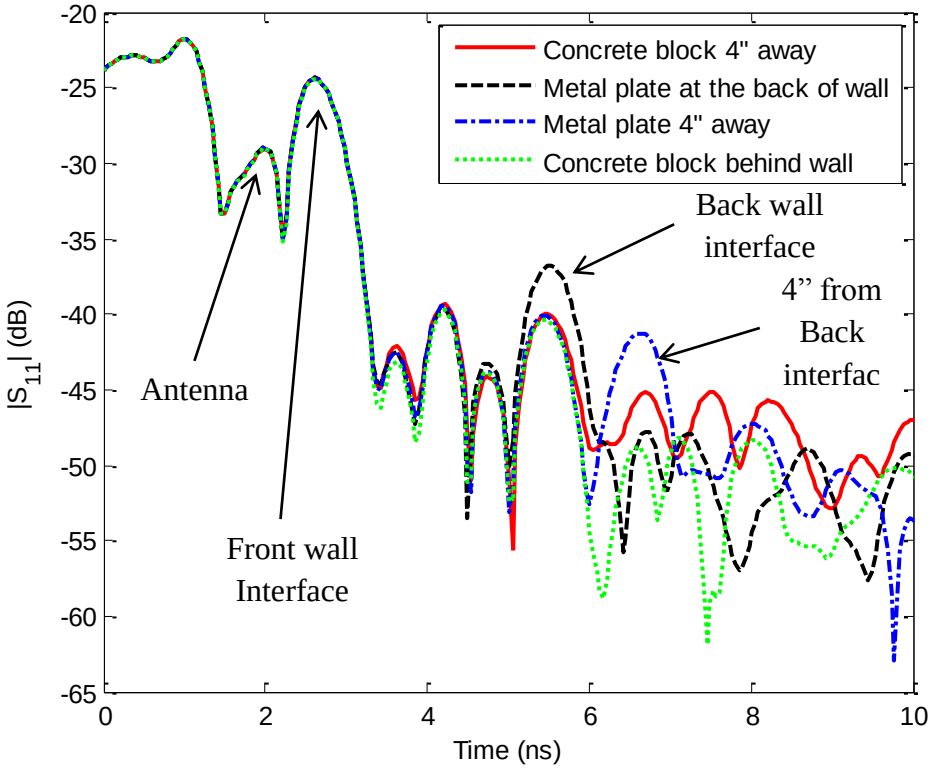

Figure 2.10 Time-domain reflectometery through the wall setup using the 1-6 GHz Vivaldi antenna

2.3 Synthetic Aperture Radar (SAR) Imaging

Three-dimensional (3D) SAR imaging involves performing wideband measurements on a two-dimensional (2D) plane parallel to the surface of the wall. This technology has become significantly more advanced during the past five years for the specific purpose of NDE imaging in both system hardware and imaging algorithm development aspects [4-7]. Figure 2.11 shows the measurement setup on a single MSE wall placed horizontally on the ground. For this purpose, an Agilent 8753E vector network analyzer (VNA) was used to make reflection measurements (S_{11}) using a wideband horn antenna. The horn antenna operated in the frequency range of 1 to 4 GHz. It was scanned on a 2D grid with a spacing of 10 cm on top of the

construction foam sheet. The sheet of foam provided a uniform and flat surface for manual scanning in the absence of an automated scanning platform. The sheet of foam was 50 mm thick, which made its dielectric properties similar to air at those frequencies. The S_{11} measurements were later phase-referenced to the aperture of the antenna by accounting for the measured characteristic of the antenna [4].

The wideband SAR imaging algorithms essentially provide a 3D image. Typically, 2D slices parallel to the scan plane (at a certain depth) can also be produced from the 3D image and displayed. Figure 2.12 shows a slice image corresponding to the surface of the sample. The non-flat surface of the sample (i.e., for decorative purposes) produces strong indications due to its significantly rough surface and relatively sharp edges. Thus, these indications are due to scattering from the grooves and peaks on the concrete surface. These grooves and peaks represented a surface roughness in the range of 20 mm to 50 mm. This level of surface roughness represents a substantial portion of the mid-band wavelength (λ_o = 120 mm) and is easily detected. Figure 2.13 shows a 2D image slice of the back surface of the MSE wall section that indicates a large metal plate with dimensions of 10" x 24", which was placed on the back surface to check whether or not the method would be able to detect it. The background of this image also shows false indications that are due to the same significantly rough surface that was mentioned above. These false indications are present in the back surface image due to the limited range resolution associated with the imaging system which is directly proportional to the limited bandwidth of the measurements. These false indications, which are relatively weak in this particular image slice, can mask indications of weak scatters such as voids that may be present behind an actual MSE wall. For example, figure 2.14 shows a 2D image slice of the same MSE wall section with a sand-filled bucket placed right at its back surface. Sand produces weaker reflections compared to

the metallic plate, and as such, its indication in the image lower intensity. In this image, the false indications from the front surface are still present in the image slice of the back surface and are comparable to the indication from the sand. The sand was saturated with water, and the resulting image is shown in figure 2.15. Wet sand produces a much higher reflection compared to dry sand, as shown by the higher intensity on the indication in figure 2.15. These experiments presented a negative situation of sand in a background of air, as opposed to air voids in sand (or backfill soil). As it will be shown later, the opposite of voids in sand is similarly detected as well.

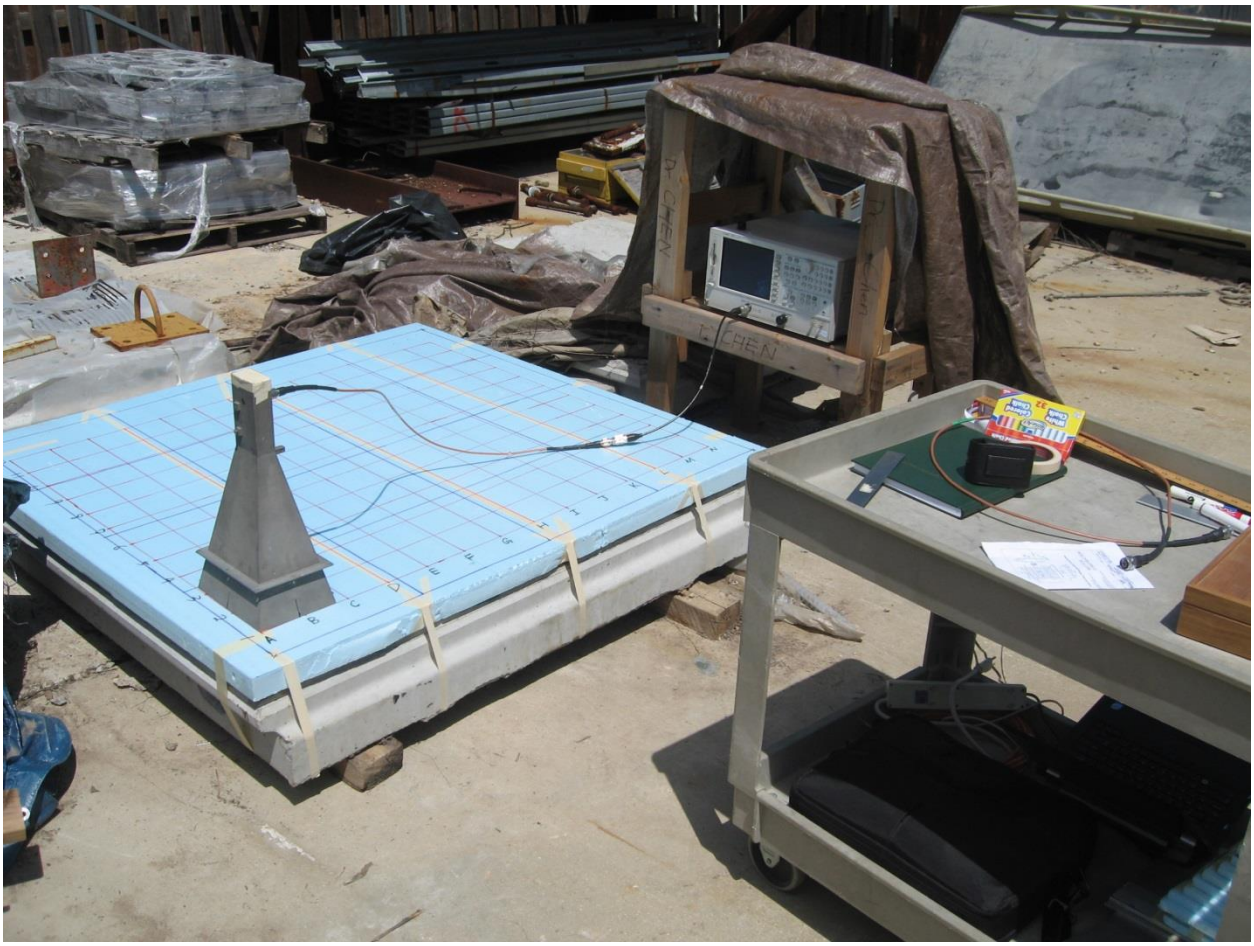

Figure 2.11 SAR imaging scan setup using a 50 mm-thick (2”) construction foam placed on top of the MSE wall section to provide a flat surface for scanning

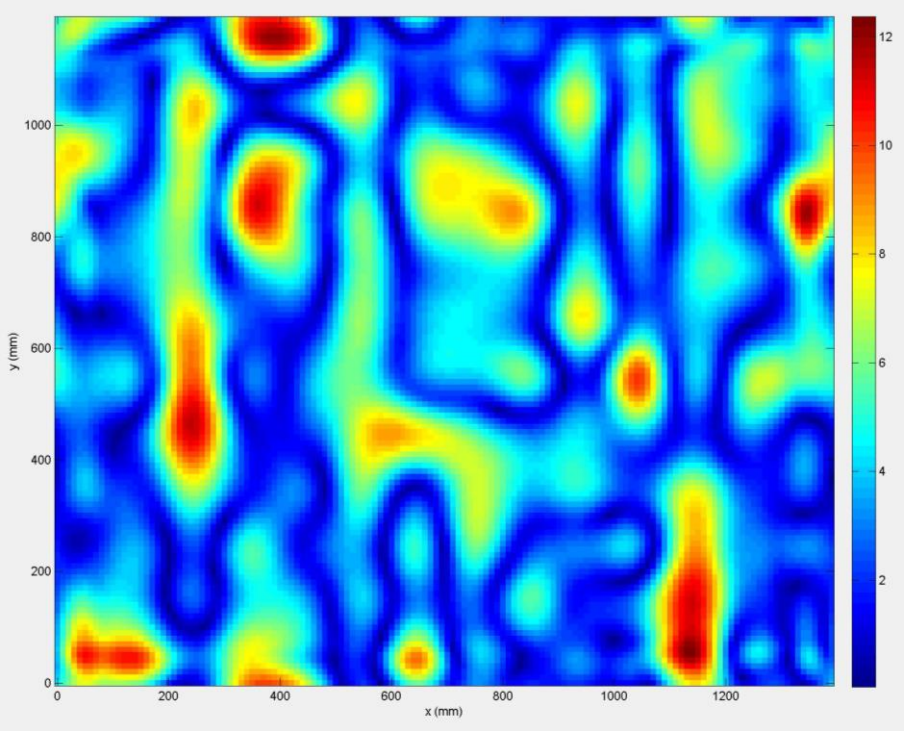

Figure 2.12 2D image slice corresponding to the surface of the MSW wall section

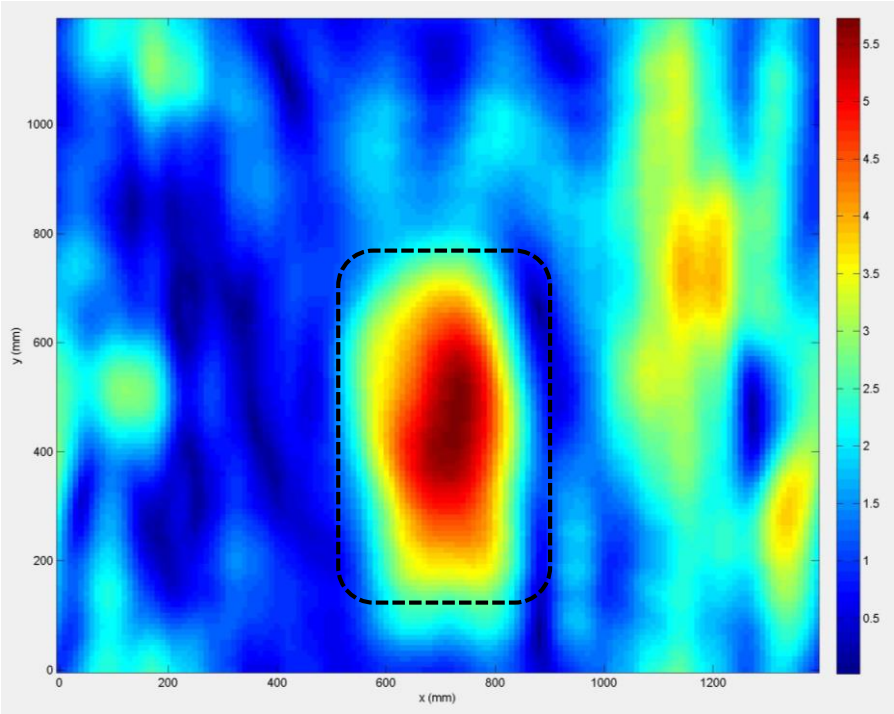

Figure 2.13 2D image slice corresponding to the back surface of the MSW wall section showing the indication of the metal plate

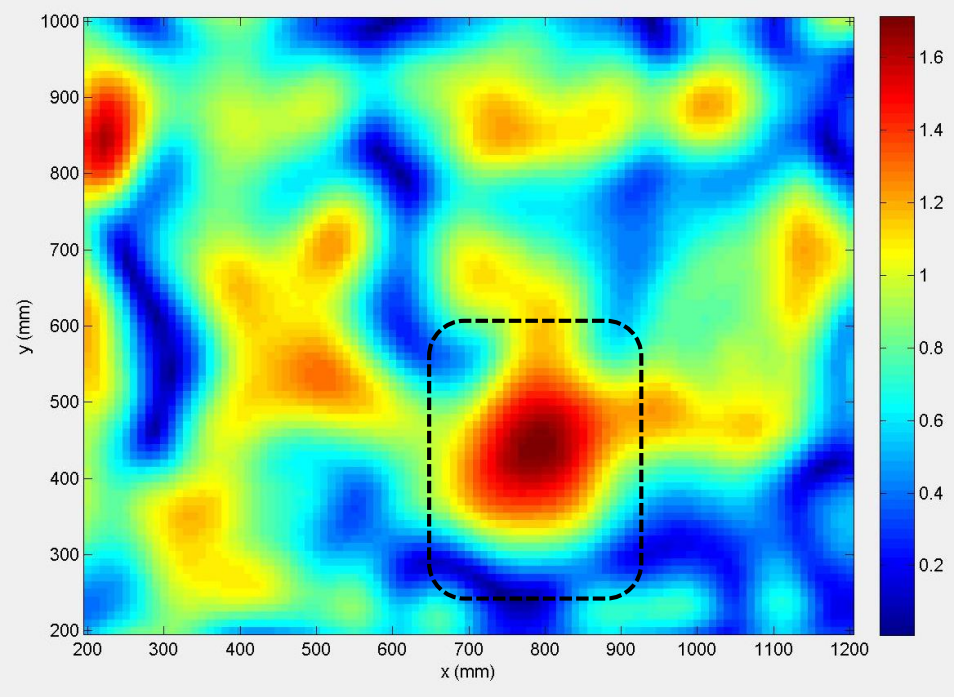

Figure 2.14 2D image slice of the back surface of the MSE wall section showing the indication of a sand-filled bucket right behind the wall section and at its back surface

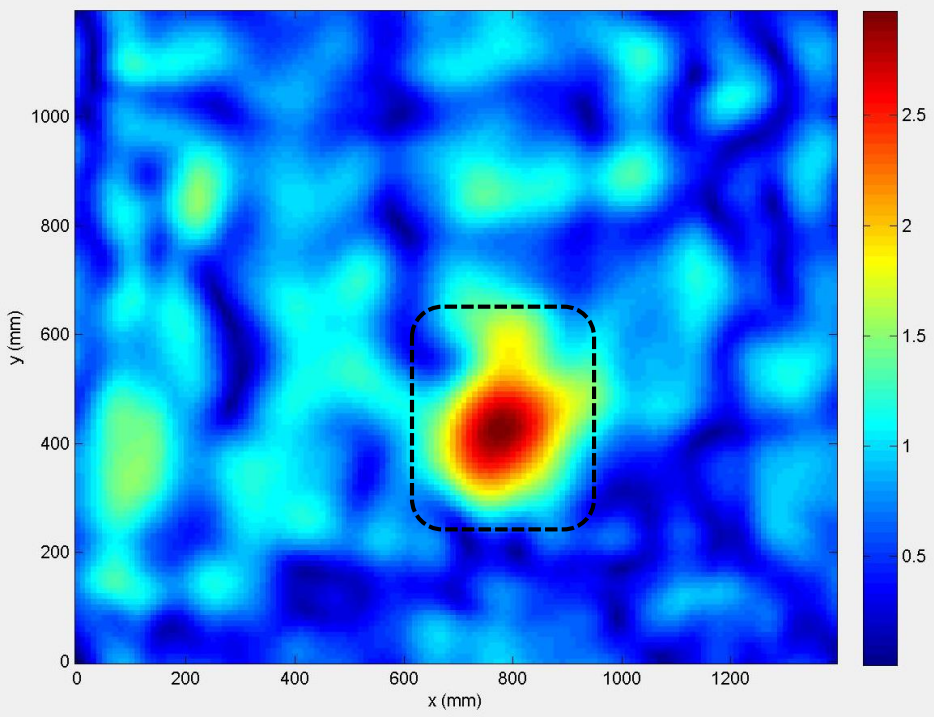

Figure 2.15 2D image slice of the back surface of the MSE wall section showing the indication of a wet sand-filled bucket

These experiments showed the potential of wideband SAR imaging for detecting voids behind an actual MSE wall with significant surface roughness. However, they also highlighted key issues to be considered when utilizing this technique for void detection. The first issue is the uneven front surface or the significant surface roughness associated with such walls. The reflections from the front surface, being very close to the antenna, are very strong when compared to reflections coming from through the thickness of the lossy concrete wall and the back surface. In the case of a wall having a uniform surface, the average reflection from across the surface can be estimated from the measured average reflection coefficient data and subsequently subtracted from the overall image data. However, in the case of this particular wall, the front surface has decorative features that are uneven and represent a substantial surface roughness. Due to this surface roughness, the reflections change greatly across the surface, and an estimate of this reflection can only be obtained from a direct point-by-point measurement prior to void development. This measurement can be made from the exact location and used for later when a void develops.

Figure 2.16 shows two image slices corresponding to the back surface of the concrete MSE wall section with and without a sand box placed behind it. This figure clearly shows the adverse effect of the surface features on detecting objects placed behind the wall since the indication of the sand box is not clearly distinguishable from the surrounding regions. Figure 2.17 shows obtained 2D slices corresponding to the front surface of the block. These images are essentially the same, signifying the repeatability of the imaging technique. When the raw measurement data of the block without the object (i.e., the sand box) is subtracted point-by-point from the raw measurement data of any subsequent scans, any fixed source of scattering, such as the surface profile and the embedded rebars, is removed. Figure 2.18 shows the image slice at the

back wall from the wall indicating the presence of the sandbox, which was obtained by subtracting a reference measurement (without the presence of sandbox). This figure clearly shows the benefit of subtracting the exact reference measurement by removing the adverse clutter due to the non-uniformity of the surface top.

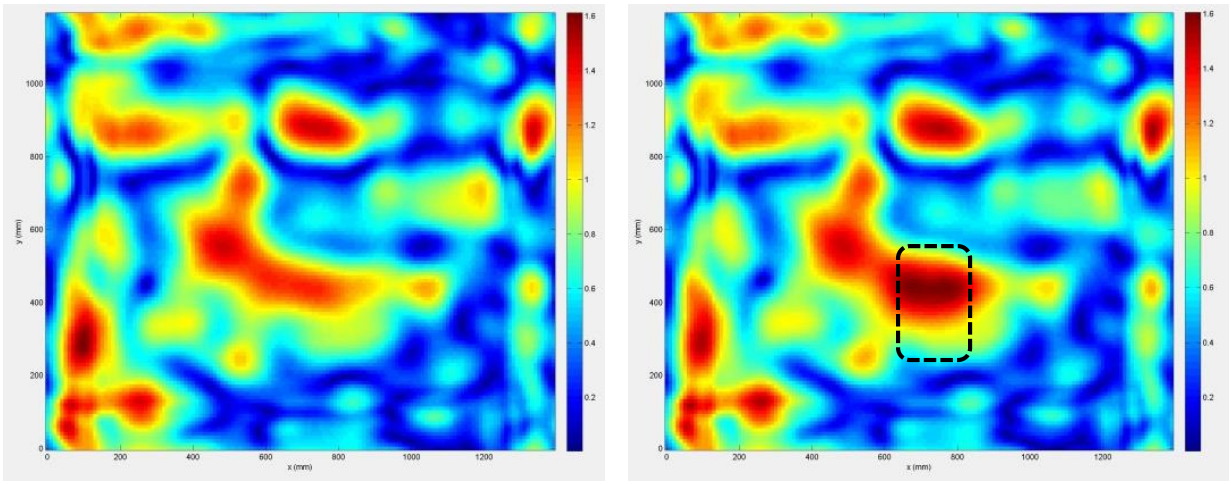

(a) (b)

Figure 2.16 2D image slice of the back surface of the concrete MSE wall section (a) without and (b) with a sand box, indicated by the dashed rectangle

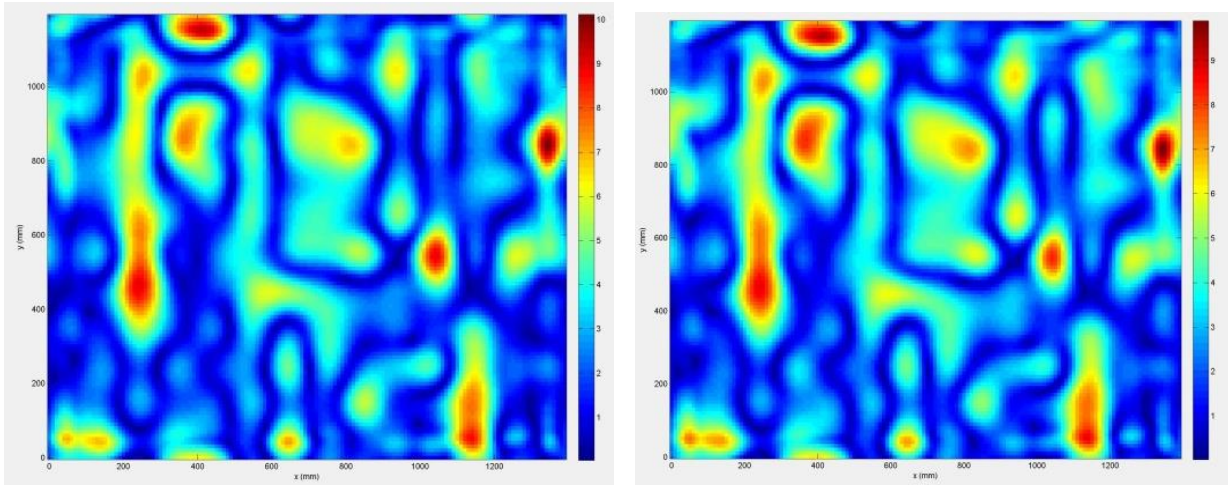

(a) (b)

Figure 2.17 2D image slice of the front surface of the concrete MSE wall section (a) without and (b) with a sand box

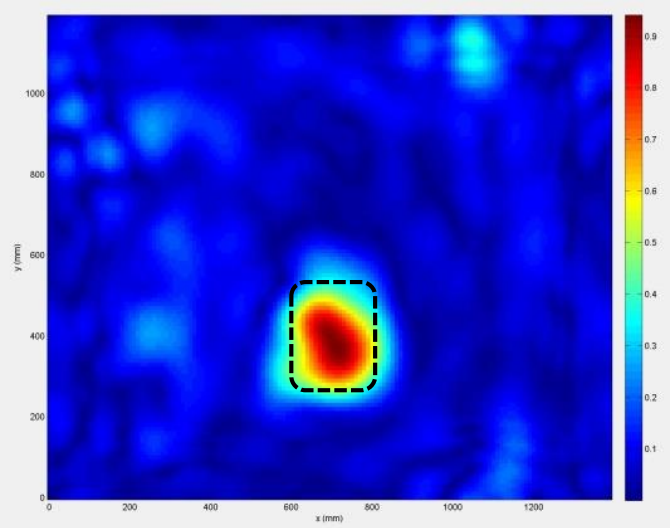

Figure 2.18 2D the back surface image slice of the concrete MSW wall section after subtraction

To further illustrate the adverse effect of surface irregularities, the grooves in the surface of a second wall section was filled in with concrete to bring the surface irregularities from ~2" to ~0.25". Subsequently, this wall section was imaged as before. Figure 2.19 shows several 2D slices at various depths within the wall section. Figure 2.19 (a) corresponds to the image slice at the wall surface. Comparing this image to that of figure 2.17, the adverse effect of surface irregularities becomes apparent. Figures 2.19 (b-c) show the image slices at the depths of vertical and horizontal rebars (10 mm deep), respectively. Note that the vertical rebars are better indicated in these images due to the fact that the polarization of the electric field (linear polarization) matches the orientation of the vertical rebars. Previously, for concrete wall sections with a strong irregular surface, the rebars were masked by the strong influence of the surface and could not be imaged. Also, subtracting a reference measurement, as illustrated above, removes the rebar indications since they are common among the different samples of the same design and/or consequent measurements of the same sample. Finally, Figure 2.19 (d) shows an image slice corresponding to the back surface of the wall where a sandbox was located. The indication

of the sandbox is better distinguishable from the background clutter in this image compared to that of figure 2.16 (b). This experiment illustrates the adverse effect of the surface irregularities in cluttering the whole volumetric image, and subsequently the image slices at depths of interest, such as the back of the concrete wall where voids are expected to be present.

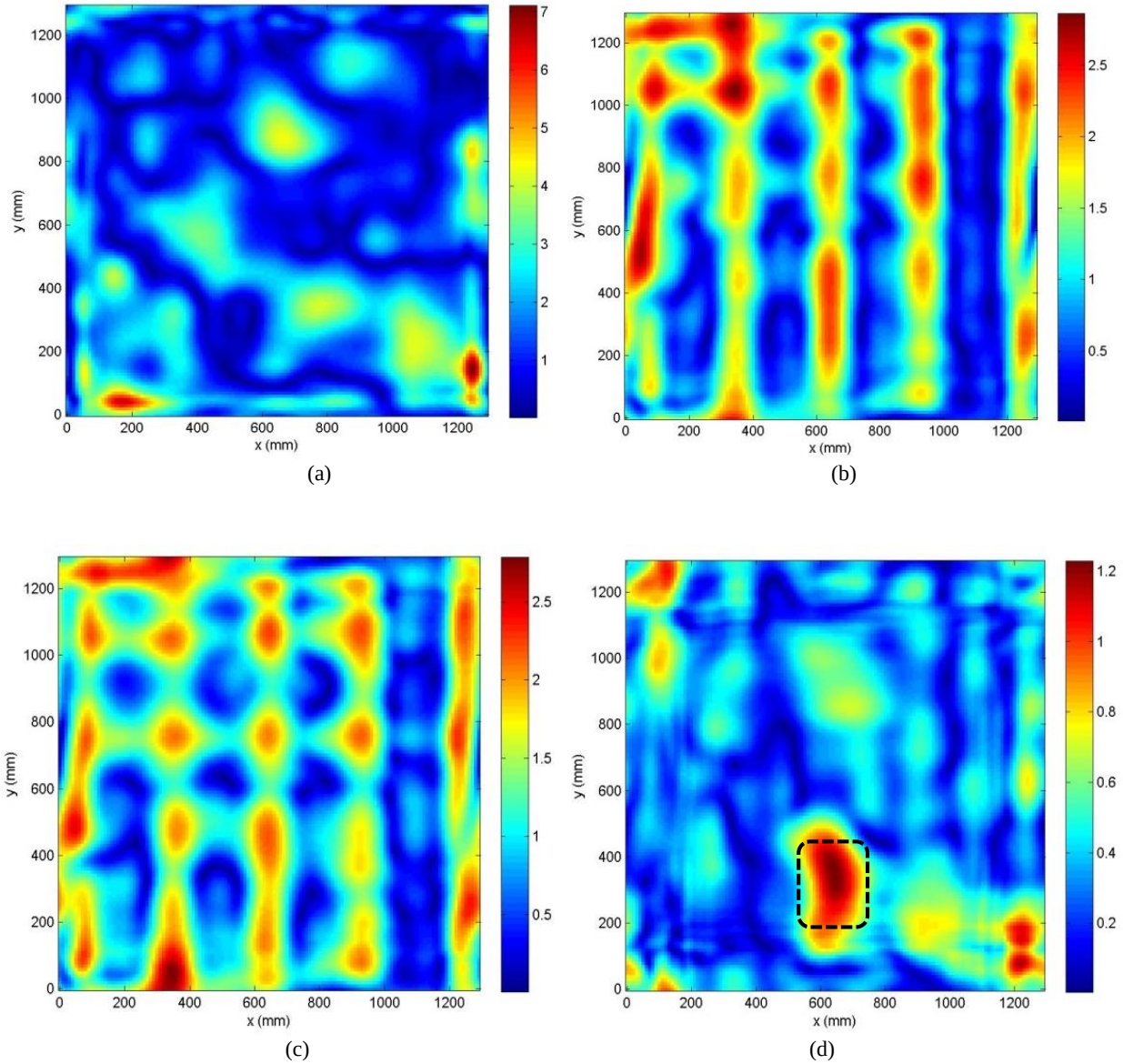

Figure 2.19 Image slices of the MSE wall section from the (a) surface of the wall, the (b) first row of rebars, the (c) second row of rebars, and the (d) surface of the back wall after filling the surface irregularities with concrete

2.4 Effect of Moisture

The intensity of the void or sand indications is directly proportional to the dielectric property contrast among the wall, sand, and air. Concrete and sand have a close relative to air (vacuum) dielectric constant (real part of dielectric property) values, (~5 for concrete and ~3 for sand) and that makes detecting air-filled voids in sand possible. On the other hand, wet sand (due to presence of water) has a much larger dielectric constant in addition to a significant loss factor (imaginary part of dielectric property). A higher level of moisture in sand will further increase the contrast between air and sand resulting in a higher contrast in the image. Furthermore, the presence of moisture will also increase the contrast between wet sand and concrete, and that will result in larger reflections from the concrete sand boundary. Figure 2.20 shows images of a sandbox placed behind the MSE wall section with a smoothed surface (filled with concrete). The first image, figure 2.20 (a), is of dry sand. For the second image, figure 2.20 (b), the sand (≈ 7700 g) was mixed with 500 ml of water. For the next two images, figures 2.20 (c-d), the moisture level was increased by 500 ml increments, respectively. For the last image, figure 2.20 (e), the sand was replaced by water. As can be concluded from these images, the signal level in the sand indication is increasing proportionally with the moisture level. An exception is the water-only case, where the intensity of the indication decreased. We believe that for the latter case, a slight air gap existed between the back surface of the concrete wall section and the water container, along with the reduced the reflections from the water. Figure 2.21 shows a summary of these results where the target intensity is calculated and plotted along with the background intensity (clutter level). This figure shows that as the moisture level increases, the intensity of the target increases, while the clutter level in the background remains constant as expected. This experiment shows that the presence of moisture enhances void detectability. However, one can expect that non-uniform wetness and pockets of water behind the wall can lead to false

indications of voids. As will be shown later, voids produce a lower reflection compared to sand and water, and therefore voids will be represented as dark spots (blue) in the image compared to water which will be represented as bright (red) spots.

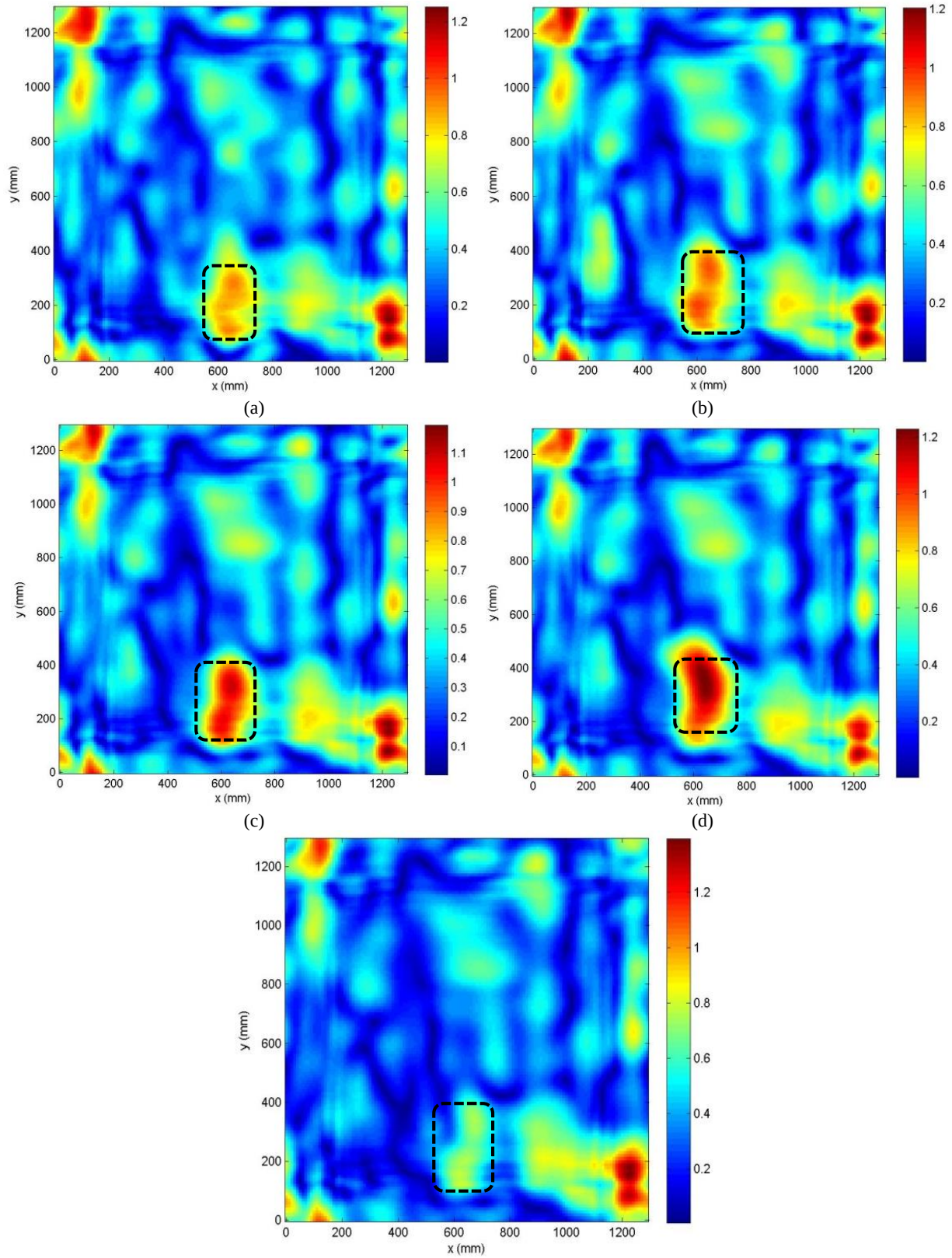

Figure 2.20 Images of the wall section after filling the surface irregularities with concrete: (a) dry sand, (b) wet sand 500 ml, (c) wet sand 1000 ml, (d) wet sand 1500 ml, and (e) water

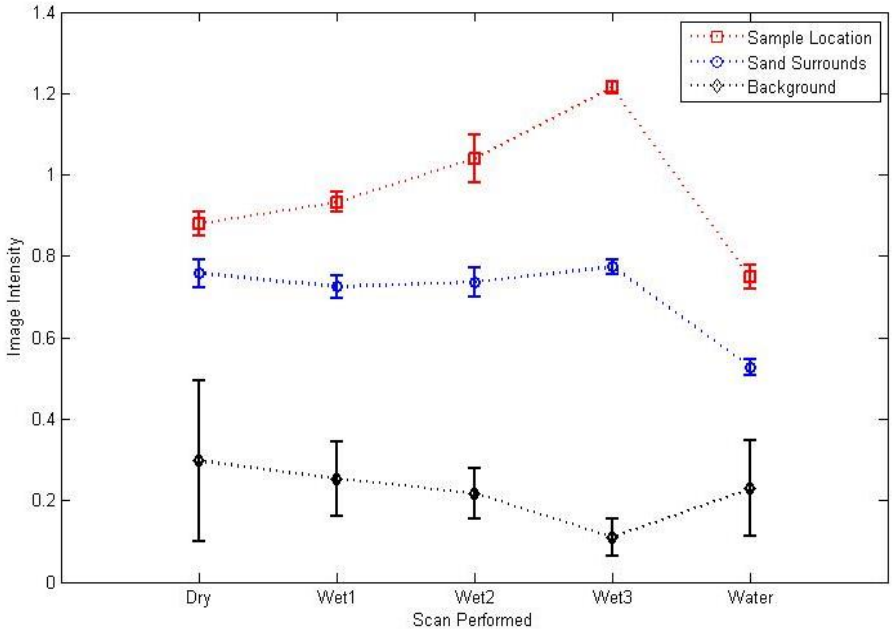

Figure 2.21 Target indication intensity compared to average background intensity

2.5 Void Detection

So far, the inverse of the void (i.e., sandbox surrounded by air) was scanned to practically show the feasibility of void detection behind a concrete wall. In this section, the results of imaging actual voids are demonstrated. A large 24”x24”x12” wooden box was constructed on top of a pallet. This large box was filled with sand, and pieces of construction foam were used to simulate voids. Foam is electromagnetically similar to air. Figure 2.22 (a) shows a 5”x5”x2” piece of foam placed inside the sand box to simulate a small void. Figure 2.22 (b) shows the sandbox placed behind a wall section using a pallet jack to move and press the sandbox to the back surface of the MSW wall section. This setup was scanned, and SAR image slices were produced as before. Figures 2.23 (a-b) shows SAR image slices at the location of the sandbox (the back surface of the wall) for a small (5”x5”x2”) and a large (10”x10”x2”) void, respectively. These images indicate the capability of SAR imaging for detecting voids in sand (or backfill soil)

behind the concrete wall. Furthermore, the size and extent of the voids are readily available in these images even through the 7”-thickness of lossy concrete. The depth of the void could not be detected due to the very limited range (depth) resolution. Nevertheless, these experiments illustrate the strength of SAR imaging in detection and the characterization of voids behind the concrete wall.

(a) (b)

Figure 2.22 (a) Large sandbox and piece of construction foam to simulate void and (b) placed behind the MSE wall section using a palette jack

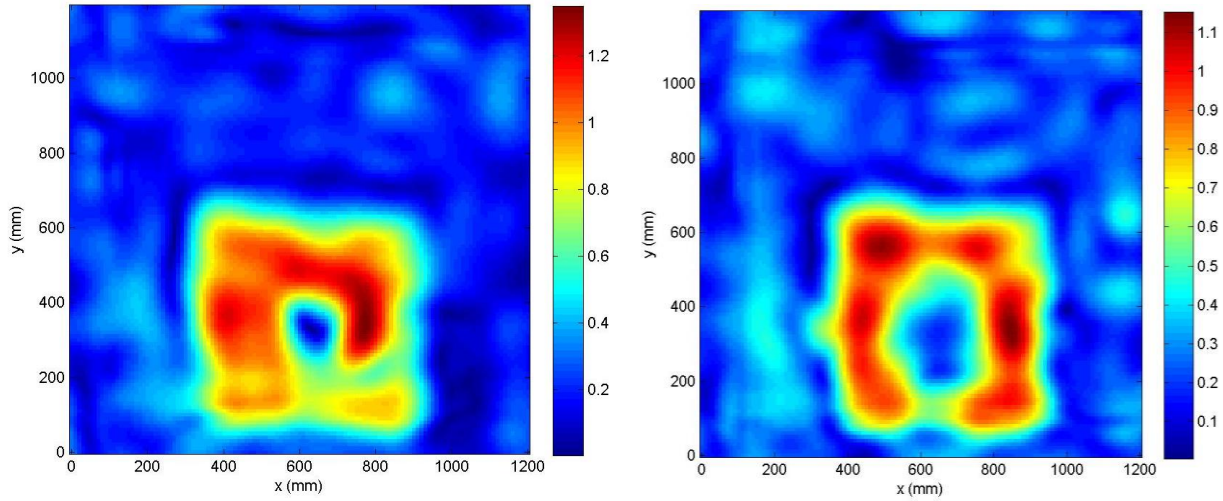

(a) (b)

Figure 2.23 Image of (a) a 5”x5”x2” void in the sandbox and (b) a 10”×10”×2” void in the sandbox

Chapter 3 Concluding Remarks

The utility of microwave NDT and many different inspection methods within this regime have shown great potential and possibilities for evaluating critical characteristics of civil infrastructures. In this study, two different wideband microwave inspection approaches were investigated for detecting and evaluating characteristics of materials behind an MSE wall section commonly used in soil retaining applications. The wall contained reinforcing steel bars both in horizontal and vertical directions and had a rough surface finishing for decorative purposes.

The first approach involved the use of a relatively high-frequency and wideband frequency-modulated continuous wave (FM-CM) radar system. It operated in an 8-18 GHz range and provided high spatial and depth (along-range) resolution. The radar system was fine tuned to enhance and improve its electrical and physical handling characteristics. While effectively operated with mortar blocks in the laboratory, the radar system had limited applications in MSE walls due to its thick layer, concrete heterogeneity, surface roughness, and the presence of steel bars. Specifically, the limited microwave penetration into the wall significantly hampered the application of the radar system in MSE walls.

Subsequently, the second approach with time-domain reflectometry was employed. The test results showed more promise since its 1-6 GHz operating frequency is much lower than that of the FM-CW radar and hence has better signal penetration capability. However, the characteristics of the wall (e.g., presence of steel bars, surface roughness, etc.) indicated that "spot type" measurements may only provide limited unambiguous measurement data/results for inspecting an MSE wall section. Therefore, 2D imaging of an anomaly was attempted. Such images allow for signal averaging and easy distinction of localized features such as steel bars from undesired flaws. To this end, a wideband laboratory imaging system (1-4 GHz) was employed along with advanced synthetic aperture radar (SAR) imaging algorithms to generate

2D slice images of the wall at different depths. This imaging approach requires scanning of the wall surface or taking measurements at many specified locations. Initially, the significant surface roughness associated with the wall limited signal penetration due to scattered signals from the rough surface. However, by using a construction foam sheet, estimating and subtracting the surface scattering, several anomalies placed behind the wall (e.g., moisture and void) were successfully detected, demonstrating the effectiveness of this imaging technique for back-fill soil inspection behind an MSE wall section. The surface scattering can be estimated from the same wall panel prior to void development and stored for future use. Alternatively, the surface scattering can be estimated from neighboring blocks. For walls that do not have any decorative surface features, this method provides better imaging capabilities.

The imaging technique also allows for distinguishing voids from water by monitoring the reflected signal strength. Voids produce less reflection compared to sand and water and appear as dark spots in the image. On the other hand, water produces a stronger reflection and appears as bright spots in the image. Further studies must be performed to properly qualify this inspection technique.

Such an imaging system can be designed to be relatively small in size and readily portable for field use, along with a scanning platform. Scanning platforms that span two neighboring wall panels can produce differential detection capabilities, further enhance the signal to clutter ratio, and potentially provide high detection probability. The microwave SAR imaging technique is robust and does not require any prior knowledge of MSE wall structure except for the thickness of walls.

References

1. Zoughi, R., L.K. Wu and R.K. Moore, "SOURCESCAT: A Very-Fine-Resolution Radar Scatterometer," *Microwave Journal*, vol. 28, no. 11, pp. 183-196, November, 1985.

2. Carroll, B. S. Kharkovsky, R. Zoughi and R. Limmer, "Frequency-modulated continuous-wave (FM-CW) radar for evaluation of refractory structures used in glass manufacturing furnaces," *in Review of Progress in Quantitative Nondestructive Evaluation Vol. 28A*, Chicago, IL, July 21- July 25, 2008, vol. 1096, AIP Conference Proceedings, edited by D.O. Thompson and D.E. Chimenti, American Institute of Physics, pp. 402-409, Melville, NY, 2009.

3. Varghese, B., C. DeConick, G. Cartee, R. Zoughi, M. Velez and R. Moore, "High-Temperature Monitoring of Refractory Wall Recession Using Frequency-Modulated Continuous-Wave (FM-CW) Radar Techniques," *Proceedings of the Thirty First Annual Review of Progress in Techniques Nondestructive Evaluation*, vol. 24B, pp. 1714-1720, Golden, Co, July 25-30, 2004.

4. Case, J.T., M.T. Ghasr, and R. Zoughi, "Optimum 2D Uniform Spatial Sampling for Microwave SAR-Based NDE Imaging Systems," *IEEE Transactions on Instrumentation and Measurement*, vol. 60, no. 12, pp. 3806-3815, December 2011.

5. Ghasr, M.T., Y. LePape, D.B. Scott, and R. Zoughi, "Holographical (3D) Microwave Imaging of Electrochemically Corroded Steel Reinforcing Bars in Concrete," *American Concrete Institute (ACI) Materials Journal*, 2014.

6. Zoughi, R., M.T. Ghasr, J.S. Popovics and S. Ham, "Comparison of Frequency-Modulated Continuous-Wave (FM-CW) Radar and Impact-Echo Data for Detecting Delamination in Concrete Bridge Decks," *Proceedings of the 40th Annual Review of Progress in Quantitative Nondestructive Evaluation Conference, American Institute of Physics*, Conference Proceedings 1581, vol. 33A, pp. 866-871, 2014.

7. Ghasr, M.T., P. Puleo, and R. Zoughi, "Novel reflectometer for millimeter wave 3D holographic imaging," *in proceedings of 2013 IEEE International Instrumentation and Measurement Technology Conference (I2MTC)*, pp.647-651, 6-9 May 2013.

Publications

1. Ghasr, M.T., Y. Bao, K. Ying, G. Chen and R. Zoughi, "Microwave SAR Imaging for Nondestructive Evaluation of Mechanically Stabilized Earth Walls," To be presented at the NDE/NDT for Structural Materials Technology for Highways and Bridges (SMT), Washington, D.C., August 24-27, 2014.
2. Ghasr, M.T., Y. Bao, G. Chen and R. Zoughi, "FM-CW Radar Application for Nondestructive Evaluation of Mechanically Stabilized Earth Walls", Presented at the American Society for Nondestructive (ASNT) Spring Conference, Memphis, TN, March 18-21, 2013.